The $Q_{1,2}$–Q_7 interference contributions to $b \to s\gamma$ at $\mathcal{O}(\alpha_s^2)$ for the physical value of m_c

M. Czaja[1], M. Czakon[2], T. Huber[3], M. Misiak[1], M. Niggetiedt[4], A. Rehman[5,6],
K. Schönwald[7] and M. Steinhauser[8]

[1] *Institute of Theoretical Physics, Faculty of Physics, University of Warsaw,
02-093 Warsaw, Poland.*

[2] *Institut für Theoretische Teilchenphysik und Kosmologie, RWTH Aachen University,
52056 Aachen, Germany.*

[3] *Theoretische Physik 1, Center for Particle Physics Siegen (CPPS), Universität Siegen,
57068 Siegen, Germany.*

[4] *Max Planck Institute for Physics, Föhringer Ring 6, 80805 München, Germany.*

[5] *Department of Physics, University of Alberta, Edmonton, AB T6G 2E1, Canada.*

[6] *National Centre for Physics, Quaid-i-Azam University Campus, Islamabad 45320, Pakistan.*

[7] *Physik Institut, Universität Zürich, 8057 Zürich, Switzerland.*

[8] *Institut für Theoretische Teilchenphysik, Karlsruhe Institute of Technology (KIT),
76128 Karlsruhe, Germany.*

Abstract

The $\bar{B} \to X_s\gamma$ branching ratio is currently measured with around 5% accuracy. Further improvement is expected from Belle II. To match such a precision on the theoretical side, evaluation of $\mathcal{O}(\alpha_s^2)$ corrections to the partonic decay $b \to X_s^{\text{part}}\gamma$ are necessary, which includes the $b \to s\gamma$, $b \to sg\gamma$, $b \to sgg\gamma$, $b \to sq\bar{q}\gamma$ decay channels. Here, we evaluate the unrenormalized contribution to $b \to s\gamma$ that stems from the interference of the photonic dipole operator Q_7 and the current-current operators Q_1 and Q_2. Our results, obtained in the cut propagator approach at the 4-loop level, agree with those found in parallel by Fael *et al.* who have applied the amplitude approach at the 3-loop level. Partial results for the same quantities recently determined by Greub *et al.* agree with our findings, too.

arXiv:2309.14707v1 [hep-ph] 26 Sep 2023

1 Introduction

Rare B-meson decays that receive the leading Standard Model (SM) contributions from one-loop diagrams provide important constraints on popular Beyond Standard Model (BSM) scenarios. Among them, the inclusive radiative decay $\bar{B} \to X_s\gamma$ is of particular interest. Its isospin- and CP-averaged branching ratio has been measured by CLEO [1], Belle [2,3], BABAR [4–6], and Belle II [7] for $E_\gamma > E_0$ in the decaying meson rest frame, with various values of E_0, ranging from $1.7\,\mathrm{GeV}$ to $2.0\,\mathrm{GeV}$. The current world average of these measurements[1] extrapolated to $E_0 = 1.6\,\mathrm{GeV}$ reads [8,9]

$$\mathcal{B}(\bar{B} \to X_s\gamma)^{\mathrm{exp}} = (3.49 \pm 0.19) \times 10^{-4}\,. \tag{1.1}$$

An extrapolation in E_0 has been applied because measurements are less precise for lower values of E_0 due to rapidly growing background — see, e.g., Fig. 2 in Ref. [7]. On the other hand, theoretical estimates of non-perturbative effects are less precise for higher values of E_0 — see Refs. [10,11] for the most recent analyses of this issue.

At $E_0 = 1.6\,\mathrm{GeV}$, the $\bar{B} \to X_s\gamma$ decay rate is well approximated by the corresponding perturbative $b \to X_s^p\gamma$ decay rate, where $X_s^p = s, sg, sgg, sq\bar{q}, \ldots$ are the partonic final states. Most relevant non-perturbative corrections to this approximation are suppressed by powers of $(m_B - m_b)/m_b$. The largest non-perturbative contribution to the overall uncertainty arises from the so-called resolved photon effects that have been extensively studied in Refs. [12–16].

As far as the dominant perturbative contributions are concerned, they need to be evaluated including Next-to-Leading Order (NLO) electroweak and Next-to-Next-to-Leading Order (NNLO) QCD corrections to match the experimental accuracy. Some of the important NNLO QCD ($\mathcal{O}(\alpha_s^2)$) corrections that depend on the charm quark mass m_c have been calculated only in the limits $m_c = 0$ [17] and $m_c \gg m_b$ [18]. Next, an interpolation between the two limits was applied [17]. The resulting SM prediction obtained in 2015 [19] was subsequently updated in 2020 [20] to yield

$$\mathcal{B}(\bar{B} \to X_s\gamma)^{\mathrm{SM}} = (3.40 \pm 0.17) \times 10^{-4}\,, \tag{1.2}$$

where the overall uncertainty contains $\pm 3\%$ from the m_c-interpolation, $\pm 3\%$ from unknown higher-order effects, and $\pm 2.5\%$ from the input parameters (combined in quadrature). Non-perturbative uncertainties are among the parametric ones, with the resolved photon contributions treated along the lines of Ref. [13] — see Ref. [20] for details.

While the results in Eqs. (1.1) and (1.2) are in perfect agreement, further improvement on both the experimental and theoretical sides are expected. The ultimate Belle II luminosity is going to allow for high-statistics measurements using the hadronic tag method for the recoiling B meson, which efficiently suppresses the non-$B\bar{B}$ backgrounds [21] and makes the determination of E_γ in the decaying B-meson rest frame possible on the event-by-event basis [4,7]. As far as the perturbative calculations are concerned, the main effort is being devoted to eliminating the m_c-interpolation at $\mathcal{O}(\alpha_s^2)$ by evaluation of the corresponding corrections at the physical value of m_c.

---

[1]The most recent Belle II result [7] is not yet included in the average (1.1).

In the current paper, we present results of our calculation of the unrenormalized m_c-dependent NNLO QCD corrections to the $b \to s\gamma$ decay rate at the physical value of m_c. They need to be supplemented in the future with the corresponding bremsstrahlung contributions (with $X_s^p = sg, sgg, sq\bar{q}$), for which our calculations are advanced but yet unfinished. However, the observed agreement with the parallel calculation of Ref. [22], as well as the published partial results of Ref. [23] makes us confident that the two-body-final-state contributions in our calculation can be treated as cross-checked, and are ready for publication.

The article is organized as follows. In the next section, we provide the necessary definitions to specify the corrections we actually calculate. Next, our method for evaluation of 4-loop propagator diagrams with unitarity cuts is briefly described. In Section 3, our final results for the considered corrections are presented for a sample physical value of $z = m_c^2/m_b^2$, namely $z = 0.04$. We conclude in Section 4.

2   Details of the calculation

We work in the framework of an effective theory that is obtained from the SM via decoupling of the W boson and all the heavier particles. The flavour-changing weak interaction terms that affect the $b \to s\gamma$ transition take then the form[2]

$$\mathcal{L}_{\text{int}} = \frac{4G_F}{\sqrt{2}} V_{ts}^* V_{tb} \sum_{i=1}^{8} C_i(\mu_b) Q_i \,. \tag{2.1}$$

The $\overline{\text{MS}}$-renormalized Wilson coefficients $C_i(\mu_b)$ are already known up to NNLO in QCD at the renormalization scale $\mu_b \sim m_b$. Explicit expressions for the operators Q_i can be found, e.g., in Eq. (1.6) of Ref. [17].[3] For our present purpose, only three of them matter, namely

$$Q_1 = (\bar{s}_L \gamma_\mu T^a c_L)(\bar{c}_L \gamma^\mu T^a b_L), \qquad Q_2 = (\bar{s}_L \gamma_\mu c_L)(\bar{c}_L \gamma^\mu b_L), \qquad Q_7 = \frac{e}{16\pi^2} m_b(\bar{s}_L \sigma^{\mu\nu} b_R) F_{\mu\nu} \,. \tag{2.2}$$

The weak radiative b-quark decay rate can be written as

$$\Gamma(b \to X_s^p \gamma) = \frac{G_F^2 \alpha_{em} m_{b,\text{pole}}^5}{32\pi^4} |V_{ts}^* V_{tb}|^2 \sum_{i,j=1}^{8} C_i(\mu_b) C_j(\mu_b) \hat{G}_{ij} \,, \tag{2.3}$$

where the quantities $\hat{G}_{ij}$ depend on the photon energy cut E_0, the renormalization scale μ_b, and the ratio $z = m_c^2/m_b^2$ of the charm and bottom quark masses.[4] Their perturbative expansion in α_s reads

$$\hat{G}_{ij} = \hat{G}_{ij}^{(0)} + \frac{\alpha_s}{4\pi} \hat{G}_{ij}^{(1)} + \left(\frac{\alpha_s}{4\pi}\right)^2 \hat{G}_{ij}^{(2)} + \mathcal{O}(\alpha_s^3) \,. \tag{2.4}$$

---

[2]Terms that matter beyond the leading order in electroweak interactions only and/or are suppressed by the small Cabibbo-Kobayashi-Maskawa matrix element V_{ub} are going to be ignored here, as we focus on $\mathcal{O}(\alpha_s^2)$ effects.

[3]We shall strictly follow the notation of Ref. [17] throughout the current paper.

[4]The light u, d and s quark masses are set to zero in $\mathcal{O}(\alpha_s^2)$ interference terms involving the operator Q_7 that are of our interest here. However, they need to be retained in numerically subleading terms to get rid of collinear divergences — see, e.g., Refs. [24, 25].

Currently, the dominant uncertainty in Eq. (2.3) arises from the z-dependence of $\hat{G}_{17}^{(2)}$ and $\hat{G}_{27}^{(2)}$. These are the very quantities for which the interpolation mentioned in the Introduction has been applied. Our discussion in the following is going to refer to $\hat{G}_{27}^{(2)}$ for brevity. The calculation of $\hat{G}_{17}^{(2)}$ has been done alongside – it differs by colour factors only. We shall present both results in Section 3.

Let us split the unrenormalized (bare) interference term $\hat{G}_{27}^{(2)\mathrm{bare}}$ into contributions from two-, three- and four-particle final states

$$\hat{G}_{27}^{(2)\mathrm{bare}} = \hat{G}_{27}^{(2)2P} + \hat{G}_{27}^{(2)3P} + \hat{G}_{27}^{(2)4P} . \tag{2.5}$$

The two-particle contribution $\hat{G}_{27}^{(2)2P}$ can be further split into a sum of two types of interferences

$$\hat{G}_{27}^{(2)2P} = \Delta_{30}\hat{G}_{27}^{(2)2P} + \Delta_{21}\hat{G}_{27}^{(2)2P} , \tag{2.6}$$

where each Δ_{kn} picks the interference of a k-loop amplitude with the insertion of Q_2, and an n-loop amplitude with the insertion of Q_7. There are only two terms in Eq. (2.6) because the one-loop $b \to s\gamma$ matrix element of Q_2 turns out to vanish.

In the next section, we are going to present separate results for $\Delta_{30}\hat{G}_{27}^{(2)2P}$ and $\Delta_{21}\hat{G}_{27}^{(2)2P}$. The former can be calculated in two possible ways. One of them is to compute the three-loop $b \to s\gamma$ matrix element of Q_2, and multiply its real part[5] by the (real) tree-level matrix element of Q_7. Such an "amplitude" approach was applied in Ref. [22]. Partial results for $\Delta_{30}\hat{G}_{27}^{(2)2P}$ in Ref. [23] were obtained using the same method, too.

Here, we apply the cut propagator approach, as it was done in Ref. [17] in the $m_c = 0$ case. It requires essentially the same effort as the amplitude approach in the case of two-particle final states, but is likely more convenient for higher-multiplicity final states. Following the well-known procedure [26], we express the phase-space integrals in terms of regular loop integrals but with cut propagators though, using the identity

$$2\pi i \delta(p^2 - m^2) = \frac{1}{p^2 - m^2 + i\varepsilon} - \frac{1}{p^2 - m^2 - i\varepsilon} . \tag{2.7}$$

Once this is done, the usual Integration-By-Parts (IBP) algorithms can be used to express the quantities in question in terms of Master Integrals (MIs). The same algorithms are applied to derive Differential Equations (DEs) for the MIs, which is essential for their efficient evaluation.

Sample four-loop propagator diagrams that contribute to $\hat{G}_{27}^{(2)2P}$ in our approach are presented in Fig. 1. Let us note that there exist physical cuts in some of these diagrams that do not go through the photon line, and therefore should not be included. This means that we neither take the imaginary part of the whole four-loop propagator, nor take advantage of the optical theorem.

We generate the necessary diagrams with the help of `QGRAF` [27] and/or `FeynArts` [28, 29] supplemented with self-written codes. The Feynman-'t Hooft gauge fixing ($\xi = 1$) is used.

---

[5]The imaginary part would matter only for the $\mathcal{O}(V_{ub})$ correction that we neglect at the $\mathcal{O}(\alpha_s^2)$ level. Such an effect drops out after CP-averaging anyway.
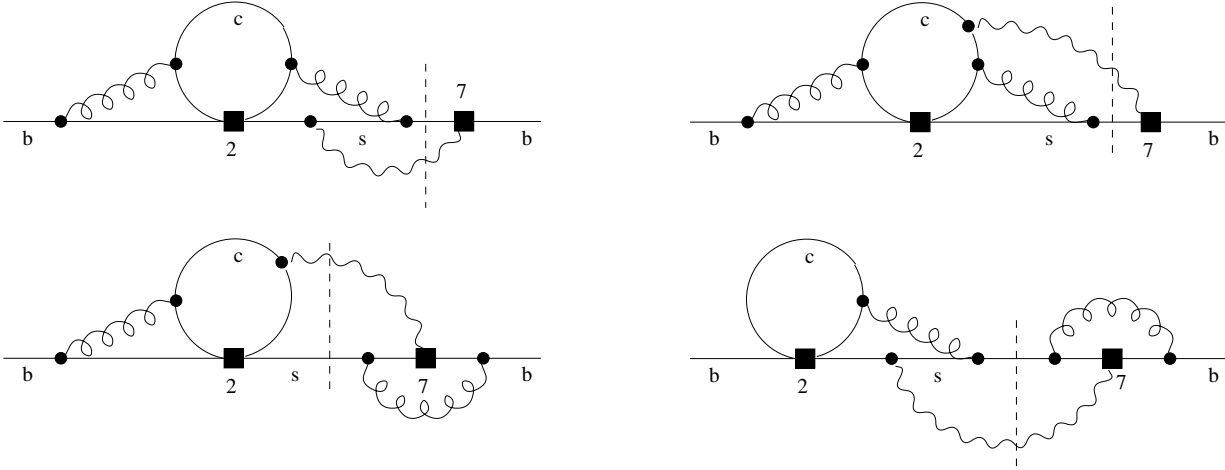
Figure 1: Sample Feynman diagrams contributing to $\Delta_{30}\hat{G}_{27}^{(2)2P}$ (upper row) and $\Delta_{21}\hat{G}_{27}^{(2)2P}$ (lower row). Black squares denote insertions of the Q_2 and Q_7 operators. The vertical dashed lines indicate which propagators are cut.

No diagrams with loop corrections on external (or cut) lines are included, which matches the conventions of the corresponding counterterm contributions in Eq. (2.1) of Ref. [30]. We skip the diagrams where no gluon connects the charm loop (with the Q_2 vertex) to the diagram remainder. Such diagrams contain subdiagrams that either vanish or sum up to zero. We also skip the diagrams with ghost or gluon one-loop corrections on the gluon lines. Their effects are read out from the corresponding massless quark loops, and included in our results in the next section. Eventually, we are left with 198 four-loop propagator diagrams that need to be calculated.

In each of the Feynman integrands, we sum over the external b-quark polarizations, and evaluate the necessary Dirac traces with the help of FORM [31]. Next, once all the Lorentz indices get contracted, the full $\hat{G}_{27}^{(2)2P}$ becomes a linear combination of scalar integrals. Their reduction to MIs is performed with the help of Kira [32,33] that generates and applies the IBP identities. Altogether, 447 MIs are found to be independent.

The calculation of MIs is performed with the help of AMFlow [34]. An artificial imaginary mass-squared parameter η is introduced in each denominator, and the IBP method is used to derive DEs in η for the MIs. Next, the DEs are numerically solved with initial conditions at very large $|\eta|$. All the physical mass ratios and dimensionless kinematical invariants are assigned fixed numerical values to facilitate the IBP reduction.

3 Results

In our case, the only physical mass ratio involved is $z = m_c^2/m_b^2$. No kinematical invariants are present, as we deal with a massive particle decay to two massless ones. To fix the numerical value of z, we follow the convention of Ref. [17] where $z = m_c^{\overline{MS}}(\mu_c)/m_{b,\text{kin}}$ was used in lower-

order contributions, where $m_{b,\text{kin}} \simeq 4.564 \,\text{GeV}$ denotes the b-quark mass in the kinetic scheme at $\mu_{\text{kin}} = 1 \,\text{GeV}$. Below, we present our final results for $z = 0.04$ that corresponds to $\mu_c \simeq m_b(m_b) \simeq 4.2 \,\text{GeV}$.

Our expressions for $\Delta_{30}\hat{G}_{27}^{(2)2P}$ and $\Delta_{30}\hat{G}_{17}^{(2)2P}$ at $z = 0.04$ read

$$
\begin{aligned}
\Delta_{30}\hat{G}_{27}^{(2)2P}(z = 0.04) \;\simeq\; & \frac{0.181070}{\epsilon^3} - \frac{6.063805}{\epsilon^2} - \frac{34.087329}{\epsilon} - 127.624515 \\
& + \left(\frac{0.482853}{\epsilon^2} + \frac{4.093615}{\epsilon} + 10.984004 \right) n_b \\
& + \left(\frac{0.482853}{\epsilon^2} + \frac{4.185427}{\epsilon} + 19.194053 \right) n_c \\
& + \left(\frac{0.482853}{\epsilon^2} + \frac{4.135795}{\epsilon} + 19.647238 \right) n_l \, ,
\end{aligned}
$$

$$
\Delta_{30}\hat{G}_{17}^{(2)2P}(z = 0.04) \;\simeq\; -\frac{1}{6}\Delta_{30}\hat{G}_{27}^{(2)2P}(z = 0.04) + \frac{0.987654}{\epsilon^2} + \frac{6.383643}{\epsilon} + 34.077780 \,, \quad (3.1)
$$

where all the numerical coefficients have been truncated at the sixth decimal place.

As far as $\Delta_{21}\hat{G}_{27}^{(2)2P}$ and $\Delta_{21}\hat{G}_{17}^{(2)2P}$ are concerned, we find

$$
\Delta_{21}\hat{G}_{27}^{(2)2P}(z) \;=\; \frac{368}{243\epsilon^3} + \frac{736 - 324 f_0(z)}{243\epsilon^2} + \frac{1}{\epsilon}\left(\frac{1472}{243} + \frac{92}{729}\pi^2 - \frac{8 f_0(z) + 4 f_1(z)}{3} \right) + p(z) \, ,
$$

$$
\Delta_{21}\hat{G}_{17}^{(2)2P}(z) \;=\; -\frac{1}{6}\Delta_{21}\hat{G}_{27}^{(2)2P}(z) \,, \quad (3.2)
$$

where $p(z = 0.04) \simeq 144.959811$. The large-$z$ expansion of $p(z)$ reads

$$
\begin{aligned}
p(z) \;=\; & \frac{138530}{6561} - \frac{3680}{729}\zeta(3) - \frac{6136}{243}L + \frac{5744}{729}L^2 - \frac{1808}{729}L^3 \\
& + \frac{1}{z}\left(-\frac{4222952}{1366875} - \frac{602852}{273375}L + \frac{34568}{18225}L^2 - \frac{532}{1215}L^3 \right) \\
& + \frac{1}{z^2}\left(-\frac{33395725469}{26254935000} - \frac{111861263}{93767625}L + \frac{156358}{178605}L^2 - \frac{172}{1215}L^3 \right) + \mathcal{O}\left(\frac{1}{z^3}\right) , \quad (3.3)
\end{aligned}
$$

with $L = \log z$. The NLO functions $f_0(z)$ and $f_1(z)$ are defined through

$$
\hat{G}_{27}^{(1)2P} = -\frac{92}{81\epsilon} + f_0(z) + \epsilon f_1(z) + \mathcal{O}(\epsilon^2) \,. \quad (3.4)
$$

Their expansions around $z = 0$ were originally found in Refs. [35] and [30], respectively. Fully analytical expressions for them in terms of harmonic polylogarithms have been recently determined in Ref. [22]. Their numerical values at $z = 0.04$ are $f_0(z = 0.04) \simeq -6.371045$ and $f_1(z = 0.04) \simeq -18.545805$.

Contributions from diagrams with quark loops on the gluon lines are present in Eq. (3.1) only. They are marked with $n_b = 1$ (bottom loops), $n_c = 1$ (charm loops), and $n_l = 3$ (light

5

quark loops). The main new results of the current paper are the remaining contributions that stem from diagrams with no quark loops on the gluon lines.

In the case of Eq. (3.1), we find perfect agreement with the results of Ref. [22], after taking into account their global normalization convention (see Eq. (10) there). To perform the comparison, we have relied on the supplementary material to that paper where deep expansions around $z = 0$ of their quantities t_2 and t_3 are given. We can also confirm the partial results of Ref. [23], once we restrict to their subset of diagrams.

In the case of our Eq. (3.2), analytical expressions for all the $\frac{1}{\epsilon^n}$ poles have been extracted from the former NLO QCD calculations of the $\langle s\gamma|Q_2|b\rangle_{2\,\text{loop}}$ and $\langle s\gamma|Q_7|b\rangle_{1\,\text{loop}}$ [36] matrix elements. They are in full agreement with our current numerical results. As far as the finite contribution $p(z)$ is concerned, it is determined for the first time here. It could not have been extracted from the NLO results because dimensionally regulated infrared (IR) divergences in $\langle s\gamma|Q_7|b\rangle_{1\,\text{loop}}$ make the so-far-unknown higher-order terms in the ϵ-expansion of $\langle s\gamma|Q_2|b\rangle_{2\,\text{loop}}$ relevant. The IR divergences are going to cancel out only after taking into account the yet uncalculated NNLO contributions from diagrams with 3- and 4-body cuts.

4 Summary and outlook

We evaluated the unrenormalized corrections $\hat{G}_{17}^{(2)2P}$ and $\hat{G}_{27}^{(2)2P}$ to the perturbative $b \to s\gamma$ decay rate. In the future, they need to be supplemented with contributions from three- and four-body final states to get rid of IR divergences. Next, they should be renormalized using counterterm contributions in Eq. (2.1) of Ref. [30] where all the necessary counterterm ingredients were calculated. We have already tested such a renormalization in our expansions around the large-m_c limit that are going to provide initial conditions for the DEs in z. The highest poles ($\frac{1}{\epsilon^3}$ and $\frac{1}{\epsilon^2}$) got properly renormalized out. However, a missing piece with $\frac{1}{\epsilon}$ divergence in the three- and four-body bare contributions was identified, and it is currently being evaluated.

Given that the complete (partial) results for $\Delta_{30}\hat{G}_{17}^{(2)2P}$ and $\Delta_{30}\hat{G}_{27}^{(2)2P}$ in Ref. [22] ([23]) agree with our findings, we have decided to present them now, and supplement with $\Delta_{21}\hat{G}_{17}^{(2)2P}$ and $\Delta_{21}\hat{G}_{27}^{(2)2P}$, even though no physical conclusion can be drawn from unrenormalized results alone. Given the complexity of the necessary calculations and the phenomenological relevance of the expected ultimate result, presenting intermediate results allows for valuable cross-checks and provides a boost for reaching the final goal.

Our results in the previous section have been presented only for a single value of z. In the case of $\Delta_{30}\hat{G}_{17}^{(2)2P}$ and $\Delta_{30}\hat{G}_{27}^{(2)2P}$, an exhaustive analysis of z-dependence can be found in Ref. [22]. As far as the remaining contributions are concerned, we are going to study their dependence on z only at the level of the fully inclusive and renormalized results for $\hat{G}_{17}^{(2)}$ and $\hat{G}_{27}^{(2)}$.

Acknowledgements

References

[1] S. Chen *et al.* (CLEO Collaboration), Phys. Rev. Lett. **87** (2001) 251807 [hep-ex/0108032].

[2] T. Saito *et al.* (Belle Collaboration), Phys. Rev. D **91** (2015) 052004 [arXiv:1411.7198].

[3] A. Limosani *et al.* (Belle Collaboration), Phys. Rev. Lett. **103** (2009) 241801 [arXiv:0907.1384].

[4] B. Aubert *et al.* (BaBar Collaboration), Phys. Rev. D **77** (2008) 051103 [arXiv:0711.4889].

[5] J. P. Lees *et al.* (BaBar Collaboration), Phys. Rev. D **86** (2012) 052012 [arXiv:1207.2520].

[6] J. P. Lees *et al.* (BaBar Collaboration), Phys. Rev. Lett. **109** (2012) 191801 [arXiv:1207.2690].

[7] F. Abudinén *et al.* (Belle-II Collaboration), [arXiv:2210.10220].

[8] Y. S. Amhis *et al.* (Heavy Flavor Averaging Group (HFLAV)), Phys. Rev. D **107** (2023) 052008 [arXiv:2206.07501].

[9] R. L. Workman *et al.* (Particle Data Group), PTEP **2022** (2022) 083C01.

[10] F. U. Bernlochner *et al.* (SIMBA Collaboration), Phys. Rev. Lett. **127** (2021) 102001 [arXiv:2007.04320].

[11] B. Dehnadi, I. Novikov and F. J. Tackmann, JHEP **2307** (2023) 214 [arXiv:2211.07663].

[12] M. Benzke, S. J. Lee, M. Neubert and G. Paz, JHEP **1008** (2010) 099 [arXiv:1003.5012].

[13] A. Gunawardana and G. Paz, JHEP **1911** (2019) 141 [arXiv:1908.02812].

[14] M. Benzke and T. Hurth, Phys. Rev. D **102** (2020) 114024 [arXiv:2006.00624].

[15] M. Benzke and T. Hurth, [arXiv:2303.06447].

[16] T. Hurth and R. Szafron, Nucl. Phys. B **991** (2023) 116200 [arXiv:2301.01739].

[17] M. Czakon, P. Fiedler, T. Huber, M. Misiak, T. Schutzmeier and M. Steinhauser, JHEP **1504** (2015) 168 [arXiv:1503.01791].

[18] M. Misiak and M. Steinhauser, Nucl. Phys. B **840** (2010) 271 [arXiv:1005.1173].

[19] M. Misiak, H. Asatrian, R. Boughezal, M. Czakon, T. Ewerth, A. Ferroglia, P. Fiedler, P. Gambino, C. Greub, U. Haisch, T. Huber, M. Kamiński, G. Ossola, M. Poradziński, A. Rehman, T. Schutzmeier, M. Steinhauser and J. Virto, Phys. Rev. Lett. **114** (2015) 221801 [arXiv:1503.01789].

[20] M. Misiak, A. Rehman and M. Steinhauser, JHEP **2006** (2020) 175 [arXiv:2002.01548].

[21] E. Kou *et al.* (Belle-II Collaboration), PTEP **2019** (2019) 123C01 [arXiv:1808.10567].

[22] M. Fael, F. Lange, K. Schönwald and M. Steinhauser, "Three-loop $b \to s\gamma$ vertex with current-current operators," CERN-TH-2023-148, P3H-23-059, TTP23-035, ZU-TH 56/23.

[23] C. Greub, H. M. Asatrian, F. Saturnino and C. Wiegand, JHEP **2305** (2023) 201 [arXiv:2303.01714].

[24] M. Kamiński, M. Misiak and M. Poradziński, Phys. Rev. D **86** (2012) 094004 [arXiv:1209.0965].

[25] H. M. Asatrian and C. Greub, Phys. Rev. D **88** (2013) 074014 [arXiv:1305.6464].

[26] C. Anastasiou and K. Melnikov, Nucl. Phys. B **646** (2002) 220 [hep-ph/0207004].

[27] P. Nogueira, J. Comput. Phys. **105** (1993) 279.

[28] J. Kublbeck, M. Bohm and A. Denner, Comput. Phys. Commun. **60** (1990) 165.

[29] T. Hahn, Comput. Phys. Commun. **140** (2001) 418 [hep-ph/0012260].

[30] M. Misiak, A. Rehman and M. Steinhauser, Phys. Lett. B **770** (2017) 431 [arXiv:1702.07674].

[31] B. Ruijl, T. Ueda and J. Vermaseren, arXiv:1707.06453.

[32] P. Maierhöfer, J. Usovitsch and P. Uwer, Comput. Phys. Commun. **230** (2018) 99, [arXiv:1705.05610].

[33] J. Klappert, F. Lange, P. Maierhöfer and J. Usovitsch, Comput. Phys. Commun. **266** (2021) 108024 [arXiv:2008.06494].

[34] X. Liu and Y. Q. Ma, Comput. Phys. Commun. **283** (2023) 108565 [arXiv:2201.11669].

[35] C. Greub, T. Hurth and D. Wyler, Phys. Lett. B **380** (1996) 385 [hep-ph/9602281].

[36] H. M. Asatrian, A. Hovhannisyan, V. Poghosyan, T. Ewerth, C. Greub and T. Hurth, Nucl. Phys. B **749** (2006) 325 [hep-ph/0605009].